Available online at www.sciencedirect.com

ScienceDirect

Ceramics International 40 (2014) 4117–4126

CERAMICS INTERNATIONAL

www.elsevier.com/locate/ceramint

Microstructural adjustment of Ni–$BaCe_{0.9}Y_{0.1}O_{3-\delta}$ cermet membrane for improved hydrogen permeation

Hyejin Kim[a,b], Boyoung Kim[a,b], Jongheun Lee[b], Kiyong Ahn[a], Hae-Ryoung Kim[a], Kyung Joong Yoon[a], Byung-Kook Kim[a], Young Whan Cho[a,b], Hae-Weon Lee[a], Jong-Ho Lee[a,*]

[a]*High-Temperature Energy Materials Research Center, Korea Institute of Science and Technology, Seoul 136-791, Republic of Korea*
[b]*Department of Materials Science and Engineering, Korea University, Seoul 136-701, Republic of Korea*

Received 14 July 2013; accepted 15 August 2013
Available online 26 August 2013

Abstract

Dense ceramic membranes are usually hybridized with an electronically conductive metallic phase to enhance their hydrogen permeation fluxes, thereby increasing the hydrogen-production efficiency of hydrogen separation membranes. Herein, the hydrogen-separation properties of membranes fabricated from cermets containing $BaCe_{0.9}Y_{0.1}O_{3-\delta}$ (BCY) as the proton-conducting ceramic phase and Ni as the electronic-conducting metal phase were investigated with respect to the compositions of the Ni–BCY mixture. Because the hydrogen permeability of a cermet membrane is seriously affected by microstructural parameters such as grain size and homogeneity of the cermet mixture used to fabricate it, we tried to optimize the microstructures and compositions of the Ni–BCY cermets by controlling their fabrication conditions. A high-energy milling process was employed to fabricate fine-grained, dense membranes that exhibited high levels of mixing homogeneity. From the adjustment of composition and microstructure of Ni–BCY composites, the hydrogen permeability of Ni–BCY cermet membranes can be significantly increased so that hydrogen fluxes of $\sim$0.76 $cm^3/(min\ cm^2)$ at 800 °C can be achieved.

Keywords: Ceramic membranes; Proton conductor; Cermets; Hydrogen permeation; High-energy milling

1. Introduction

Current global concerns regarding the depletion of fossil fuels and the resultant efforts to increase energy security have increased the demand for new energy carriers [1]. Several studies have investigated the possibility of replacing conventional fossil fuels with alternative energy sources such as solar, biomass, hydro, and nuclear power over the coming decades [2,3]. Hydrogen is one of the most attractive alternative energy sources that can replace fossils fuels because it is one of the cleanest fuels known and is also one of the most abundant elements on earth [4,5]. Hydrogen has been used for many industrial applications, including in polymer electrolyte membranes fuel cell (PEMFCs), solid oxide fuel cell (SOFCs), and hydrogen-fueled vehicles [6]. Because of the increased demand for hydrogen in today's industry, it has become extremely important to be able to supply ultrapure hydrogen at reasonable prices [7].

Hydrogen can be extracted from hydrogen-rich materials such as natural gas, water, or coals [8]. Among them, most of the hydrogen produced is via the steam-assisted reformation of methane [9,10]. However, this reformation process, which is performed at temperatures greater than 800 °C, creates carbon monoxide as an unwanted byproduct. Hence, considerable additional energy is required to separate and purify the hydrogen produced. Currently, pressure swing adsorption (PSA) is the most common process for separating hydrogen with a high degree of purity. This process can provide hydrogen with a wide range of purities, but the operating costs associated with PSA are extremely high [11–13]. Among the various hydrogen-separation systems available, those using membranes are among the most attractive, because these systems result in higher hydrogen conversion efficiencies and lower energy consumption. The principle behind using a hydrogen-separation membrane is relatively simple: hydrogen

*Corresponding author. Tel.: +82 29585532.
E-mail address: jongho@kist.re.kr (J.-H. Lee).

0272-8842/$ - see front matter © 2013 Elsevier Ltd and Techna Group S.r.l. All rights reserved.
http://dx.doi.org/10.1016/j.ceramint.2013.08.066

permeates across the membrane owing to a gradient in the hydrogen partial pressure across a properly sealed, impermeable barrier, with no external electrodes, circuitry, or power supplies [14].

Several different types of hydrogen-separation membranes have been proposed, including those based on dense metals and polymers, as well as microporous ones based on ceramics [5,15]. Dense polymeric membranes have the advantage of being low cost. However, they can normally be used only over a limited range of temperatures, because their thermal stability is poor. They also exhibit relatively low hydrogen selectivity. On the other hand, dense metal membranes have higher hydrogen permeability and selectivity. According to the US Department of Energy (DOE), a hydrogen flux of 124 $cm^3/(min\ cm^2)$ could be achieved using a Pd–Cu alloy foil at 400 °C [16]. However, owing to the high cost of Pd alloys, Pd–Cu alloy foils are usually employed only in the form of thin films on porous, scaffold-like substrates for increasing the hydrogen flux and decreasing the membrane price [17]. Dense ceramic membranes based on mixed ionic-electronic conductors (MIECs) are an alternative means for the simple and efficient separation of hydrogen with high selectivity at high temperatures [18]. In particular, MIEC membranes based on proton-conducting oxides transport both protons and electrons at the same time and are thus expected to exhibit high hydrogen permeability [19].

In recent years, extensive research has been performed at the Argonne National Laboratory (ANL) on the development of MIECs for use in hydrogen separation [20]. Initially, the research focused primarily on proton-conducting perovskite-structured oxides (ABO_3) such as yttrium-doped $BaCeO_3$ (BCY), which exhibits the highest known proton conductivity [21]. However, such oxides were not sufficient for achieving the desired hydrogen fluxes because the electronic conductivity of these oxides decreases in the presence of hydrogen or water vapor, resulting in the mixed conductivity being insufficient for achieving high hydrogen fluxes in the nongalvanic mode [22–27]. Hence, various cermet (ceramic–metal composite) membranes are being investigated, with additional electronic conductors being introduced in the membranes to increase their mixed conductivity [28,29].

The incorporation of a metal phase in an MIEC membrane generally enhances not only the electronic conductivity of the membrane but also its interfacial catalytic activities [30]. Till date, researchers at the ANL have tested three combinations of materials as cermets for fabrication hydrogen-separation membranes [30]: (1) a metal with low hydrogen permeability in combination with a highly proton-conducting oxide; (2) a metal or an alloy with high hydrogen permeability together with a nonproton-conducting ceramic; and (3) a combination of a hydrogen-permeable metal and a proton-conducting ceramic. According to their report on cermet membranes based on $BaCe_{0.8}Y_{0.2}O_3$ [30], hydrogen permeation through a membrane based on combination 1 is higher than that through single-phase BCY because of the contribution of the metallic phase, which increases the overall electronic conductivity. Membranes based on combination 2, which are composed of a hydrogen-permeable metal such as Pd, exhibit the highest hydrogen flux. However, even though they have attained the highest hydrogen flux, the cost problem of Pd-based metal is still remained. On the other hand, membranes based on combination 3 have been found to exhibit relatively moderate hydrogen permeability because they do not fully exploit the characteristics of the proton-conducting ceramic and the metal phase, which can further increase the degree of hydrogen permeation via ambipolar diffusion [31]. In numerous such membranes, a significant portion of hydrogen transport still takes place not by the ambipolar diffusion but by the atomic diffusion through the metallic phase. This limited occurrence of ambipolar diffusion through the cermet membrane is because of the nonoptimized microstructure of the composite used. In the case of membranes based on combinations 1 and 3, because of the highly refractory nature of proton-conducting ceramics, sintering at high temperatures is usually required to obtain membranes with fully dense bodies. When such membranes are sintered at high temperatures, the metallic phase readily agglomerates and is sometimes exuded from the membrane, resulting in a loss in the mixing homogeneity or uniformity of the cermet microstructure. Hence, in this study, to improve the microstructural homogeneity of cermet membranes (non-Pd-based combination 3 membranes), we developed a viable fabrication method based on high-energy milling that allowed homogeneous mixing of a ductile material with a brittle ceramic material [32,33].

High-energy milling processes have been primarily used for mixing ductile metals with brittle ceramics. According to the underlying theory of high-energy milling [32], when a ductile metal is mixed with a brittle oxide via high-energy milling, the particles of the ductile metal get flattened by the ball–powder–ball collisions, while those of the brittle oxide or intermetallic particles, get fragmented/comminuted. This results in the particles of the brittle oxide getting dispersed within the matrix of the ductile metal. Such a dual-phase configuration is advantageous for the following two reasons: (i) it refines the composite's microstructure; and (ii) it increases the composite powder's sinterability because more active surfaces are exposed during the high-energy milling process. Similar results were expected when a relatively soft phase (NiO) and a brittle phase (BCY) were mixed and the mixture was subjected to high-energy milling. Recently, we have shown the usefulness of the high-energy milling process to secure the microstructural homogeneity and good sinterability compared with conventional mechanical mixing [34]. According to our study, high-energy milling process was fairly efficient to fabricate the fine-grained dense membrane with an excellent level of mixing homogeneity [34].

10 mol% yttrium-doped barium cerate (BCY) was selected as a proton conducting ceramic phase because BCY exhibits protonic conductivity and sinterability higher than those of any other reported proton conductors [21,30]. Even though the stability of BCY under CO_2- and H_2O-containing atmospheres is pointed out, BCY-based cermet membrane has shown fairly stable performance up-to 80 h [35]. Nickel was selected as the metal phase for the cermet membranes owing to the following facts: (1) Ni is a well-known catalyst for the anodes in fuel cells; (2) Ni exhibits excellent chemisorption properties—these aid the catalytic reaction that takes place at the surfaces of the

membranes; [36] (3) Ni has a thermal expansion coefficient of $13.4 \times 10^{-6}\ K^{-1}$, close to that of $BaCe_{0.8}Y_{0.2}O_3$ ($11.7 \times 10^{-6}\ K^{-1}$); (4) Ni has a relatively high melting point (1453 °C), necessary to densify the membranes at high temperatures; (5) it is cheaper than Pd, which has normally been used in membranes based on the combination 3 mentioned above; (6) it is moderately permeable to hydrogen; and (7) it exhibits superior chemical and thermal stability, as well as compatibility with the BCY phase, with respect to the conditions under which nongalvanic hydrogen-separation membranes typically operate [37,38].

In this study, we optimized the compositions and microstructures of Ni–BCY composites by identifying the relation between the microstructures of the Ni–BCY composites and their hydrogen permeability. This was done to increase the protonic and electronic conductivities of the hydrogen-separation membranes fabricated from the composites so that higher levels of hydrogen permeation could be achieved.

2. Experimental

2.1. Fabrication of the Ni–Ba ($Ce_{0.9}Y_{0.1}$) $O_{3-\delta}$ cermets

Fig. 1 shows the complete procedure for fabricating the dual-phase Ni–Ba($Ce_{0.9}Y_{0.1}$)$O_{3-\delta}$ cermet membranes. The Ni–BCY powders were prepared by the solid-state reaction method. We prepared Ni–BCY cermet membranes containing Ni in three different concentrations (30, 35, and 40 volume ratio) in order to examine the effect of the compositions on the membranes of their hydrogen permeation property. Stoichiometric amounts of $C_2H_6Ni_5O_{12} \cdot 4H_2O$ (99%; Sigma Aldrich), $BaCO_3$ (Cerac; 99.9%), CeO_2 (High Purity Chemical; 99.9%), and Y_2O_3 (High Purity Chemical; 99.99%) were mixed in ethanol along with zirconia balls for 24 h. The resultant mixture was then dried over a hot plate, sieved with a 150 mesh, and then calcined at 1000 °C in air for 10 h to allow the perovskite BCY phase to form and eliminate the residual carbonates. The calcined powder was then ball-milled for 48 h to disintegrate the agglomerates present in it. In order to obtain a more homogeneous NiO–BCY composite powder, the ball-milled powder was again milled using high-energy milling (Pulverisette 6, Fritsch) for 10 h. Next, the composite powder was heat-treated at 800 °C in a mixture of 4% H_2/balance Ar for 2 h to reduce the NiO phase of the powder to a metallic Ni phase. The reduction temperature of 800 °C was determined from the results of high-temperature X-ray diffraction (XRD) analyses performed in an atmosphere of 4% hydrogen/balance Ar over temperatures ranging from 500 to 800 °C. After every fabrication step shown in Fig. 1, the phases and morphology of the sintered or reduced powder were determined using XRD analysis (PW3830, PANalytical, the Netherlands) and scanning electron microscopy (SEM), performed using an instrument equipped with an energy-dispersion X-ray spectroscopy (EDS) system.

Next, disk-type cermet membranes were prepared by the cold isostatic pressing of the Ni–BCY composite powders at 200 MPa. In order to determine the proper conditions for the

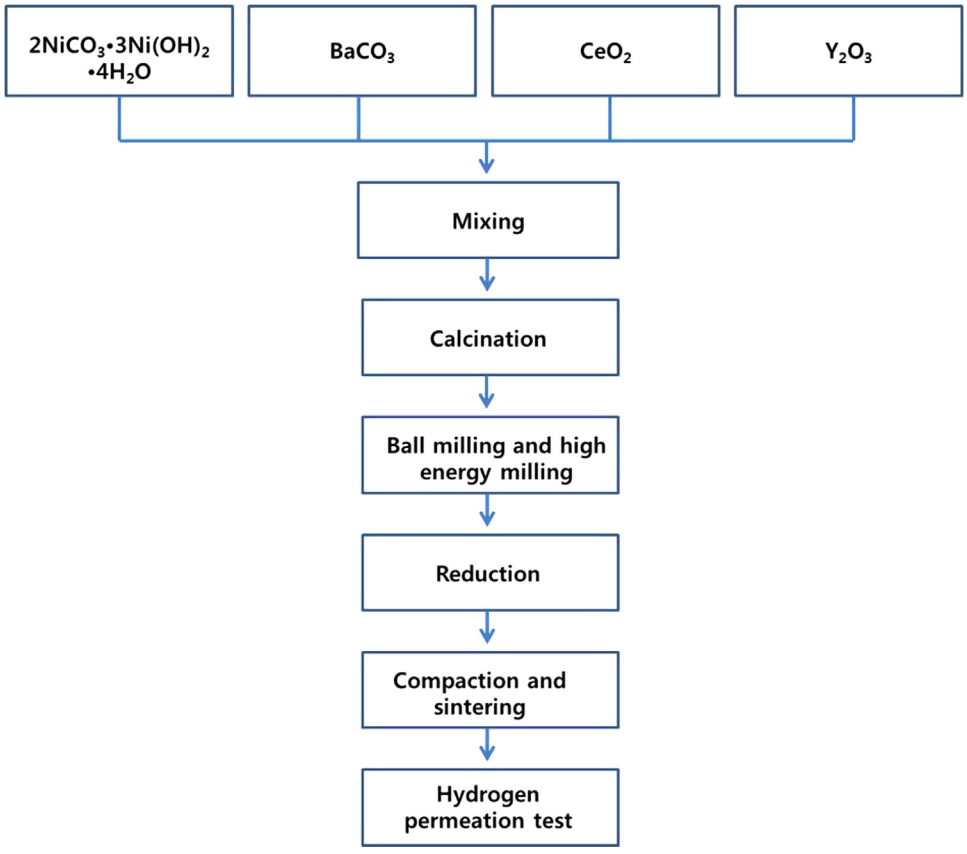

Fig. 1. Process for fabricating the Ni–BCY cermet membranes for hydrogen separation.

sintering of the Ni–BCY compacts, the sintering behaviors of the Ni–BCY powders in a reducing atmosphere were analyzed over the temperature range 25–1500 °C using a DIL 402C dilatometer with the heating rate 5 °C/min. On the basis of the results of the dilatometry analysis, the cermet membranes were sintered at 1400 °C for 10 h in a reducing atmosphere of a mixture of 4% H_2/balance Ar to prevent the reoxidation of Ni. The relative densities of all sintered samples were determined using the Archimedes' method and found to be $>98\%$. The microstructure and phases of the sintered Ni–BCY membranes were also analyzed using SEM and EDS (FEI XL-30, Philips, the Netherlands).

2.2. Characterization of Ni–BCY cermets

The electrical conductivities of the Ni–BCY composites were measured by the direct current (dc) four-probe method in the atmospheres of dry and wet hydrogen over the temperature range 200–800 °C. The electrical conductivities were measured with a current sourcemeter (KE6220, Keithley, USA) and a digital multimeter (KE2000, Keithley, USA). The hydrogen permeation property of the cermet membranes were determined using the setup shown in Fig. 2. Dense disks of the cermets (~98% of theoretical density, 17 mm in diameter) were used as the membranes. The surfaces of the membranes were polished with SiC paper of 800–2000 grits and the membranes were then affixed to the measurement tube shown in Fig. 2. The membranes were then sealed with a glass-based composite seal gasket (inner diameter: 10 mm outer diameter: 17 mm Before the commencement of the permeation tests, the samples were heated and held at 800 °C overnight to stabilize the measurement setup, including the seals formed, and to equilibrate the membrane surfaces with the surrounding atmosphere. During the permeation tests, which were performed over temperatures of 700–800 °C, a mixture of 100 ppm dry H_2/balance N_2 was used as the sweep-side gas and a mixture of 4% H_2/balance He was used as the feed gas. The flow rate of the sweep and feed gases during the permeation measurements was kept at 100 sccm using a mass flow controller, and the flow rate was measured with a flow calibrator (Field Cal 570, Humonics). The hydrogen content in the permeated stream was determined using a gas chromatograph (CP-4900 Micro GC, Varian). All the data were collected under steady-state conditions (i.e., 1 h after the temperature being investigated had been reached). Gas leaks owing to the formation of incomplete seals were detected by monitoring the permeated helium concentration in the sweep side gas and were found to account for less than 0.1% of the obtained data.

3. Results and discussion

3.1. Characterization of the Ni–BCY cermet powders

Typical XRD patterns of the NiO–BCY powders (Ni40–BCY60) after calcination at 1000 °C are shown in Fig. 3. As can be seen from the figure, a single perovskite-structured

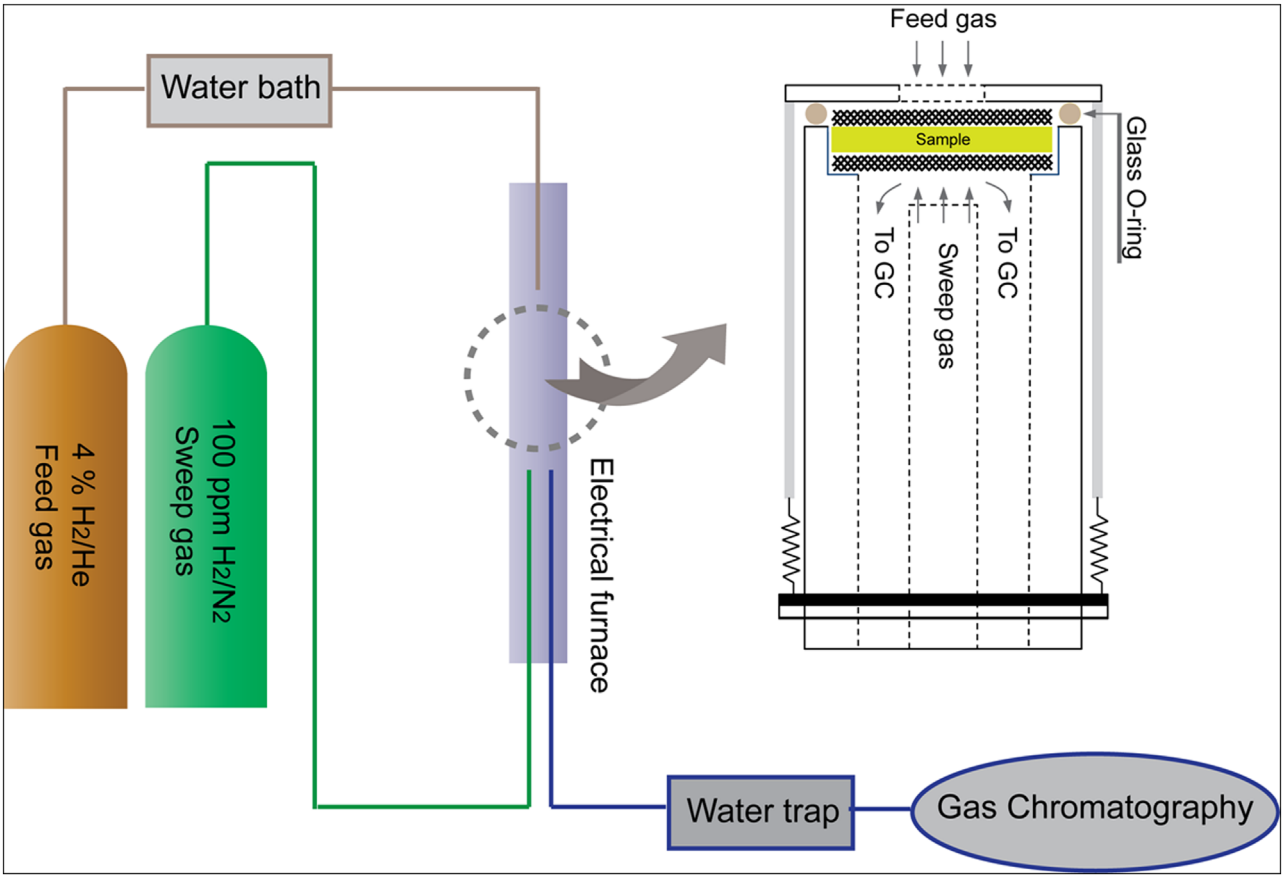

Fig. 2. Schematic of the setup used to characterize the hydrogen permeation membranes.

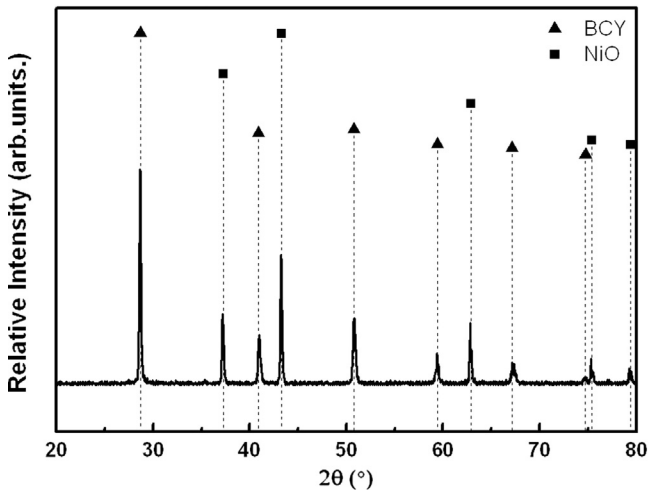

Fig. 3. X-ray diffraction pattern of a NiO–BCY powder (Ni40–BCY60) after it had been calcined at 1000 °C.

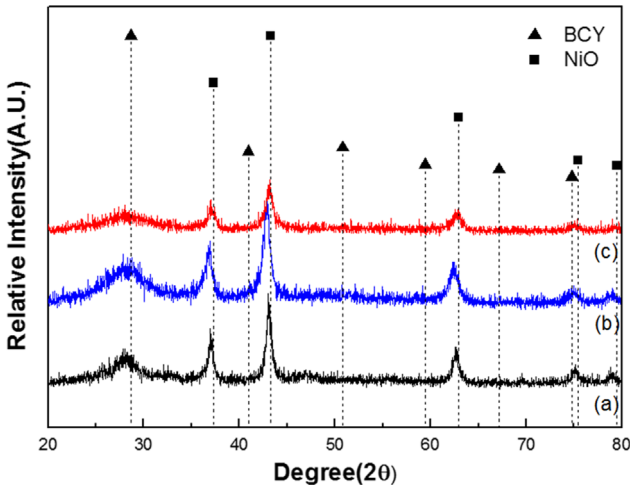

Fig. 4. X-ray diffraction patterns of various NiO–BCY powders after they had been subjected to high-energy milling for 10 h (a) Ni30–BCY70, (b) Ni35–BCY65, and (c) Ni40–BCY60.

BCY phase and a NiO phase were successfully formed after the calcination at 1000 °C with no secondary phases being present. The same results were obtained for other compositions (Ni30–BCY70 and Ni35–BCY65), indicated that the 1000 °C was the suitable calcination temperature to form the single phase BCY and NiO.

The NiO–BCY composite powders were subjected to high-energy milling to make them finer and more uniform so that the mixing of the particles of the relatively soft NiO phase and the brittle BCY phase would be more homogenous. Fig. 4 shows the XRD patterns of the NiO–BCY powders after they had been milled for 10 h. In contrast to the patterns in Fig. 3, the diffraction lines for all the compositions broadened considerably after high-energy milling. This was due to the decrease in the size of the crystallites of the powders which would be beneficial to refine the microstructure of Ni–BCY cermets.

Fig. 5 shows typical SEM micrographs of the Ni40–BCY60 powder before and after it was subjected to high-energy

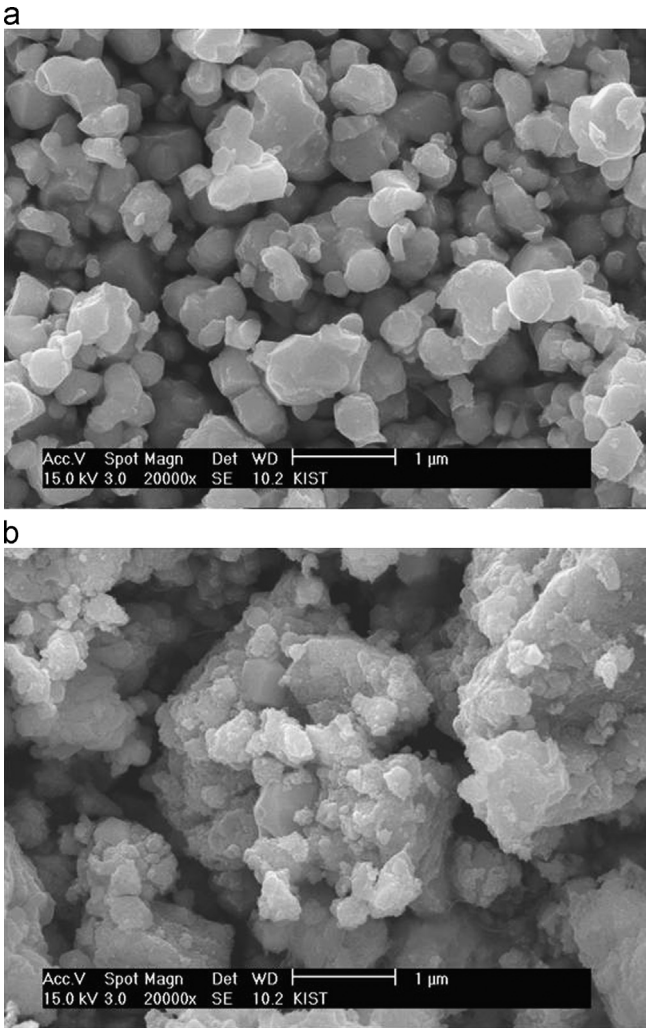

Fig. 5. SEM micrographs of NiO–BCY (Ni40–BCY60) powder (a) before and (b) after it had been subjected to high-energy milling for 10 h.

milling. As can be seen from the figure, NiO constituted the matrix phase and BCY the dispersed phase after the high-energy milling process. Using EDS analyses (see Fig. 6), it was confirmed that that brittle BCY particles coexisted with ductile NiO particles, owing to high-energy milling, in all three compositions. This confirmed the validity of using high-energy milling process for our initial purpose to make composite particles of the brittle oxide dispersed within the matrix of the ductile oxide.

To determine the optimum reduction temperature for the NiO–BCY powders, we performed in situ high-temperature X-ray analyses at temperatures of 500–800 °C in a mixture of 4% H_2/balance Ar. As shown in Fig. 7, the BCY phase decomposed and NiO phase remained unreduced after the powders were heated to 500–700 °C, indicating that these temperatures were not sufficient to reduce the NiO phase. This result also proved that the BCY powders were not stable at these temperatures. Alternatively, pure, single-phase BCY was obtained at 800 °C, with NiO being completely reduced to Ni. On the basis of these results, we set the reduction temperature for all the NiO–BCY powders to 800 °C. Fig. 8 shows the

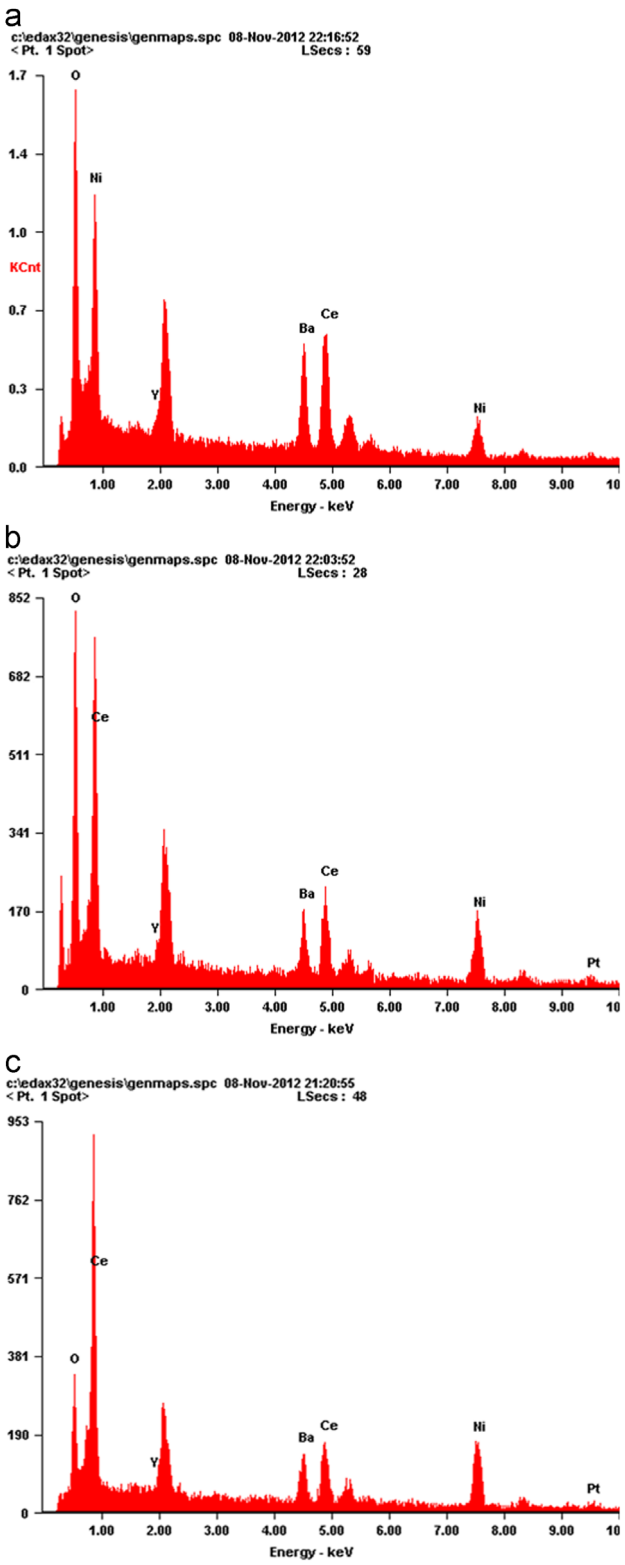

Fig. 6. EDS spectra of NiO–BCY powders after they had been subjected to high-ergy milling for 10 h: (a) Ni30–BCY70, (b) Ni35–BCY65, and (c) Ni40–BCY60.

XRD patterns of the different NiO–BCY powders after they had been completely reduced at 800 °C to the corresponding Ni–BCY powders. As can be seen from Fig. 8, all the samples

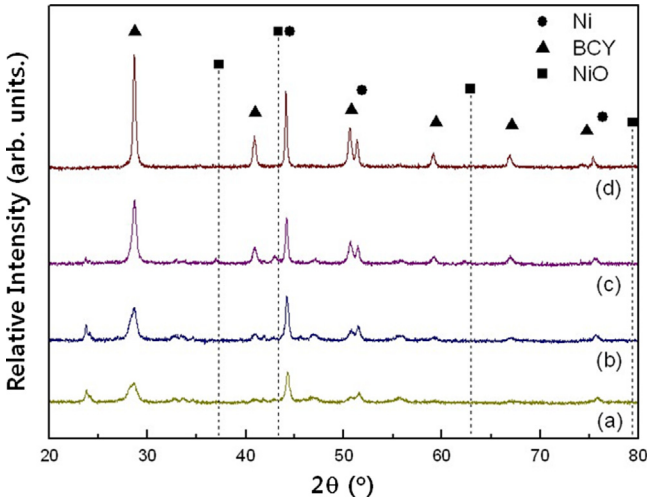

Fig. 7. X-ray diffraction patterns of NiO–BCY (Ni40–BCY60) cermets after they had been heated in a reducing atmosphere at (a) 500 °C, (b) 600 °C, (c) 700 °C, and (d) 800 °C for 2 h. (Most of non identified peaks attributed to $BaCO_3$ phase).

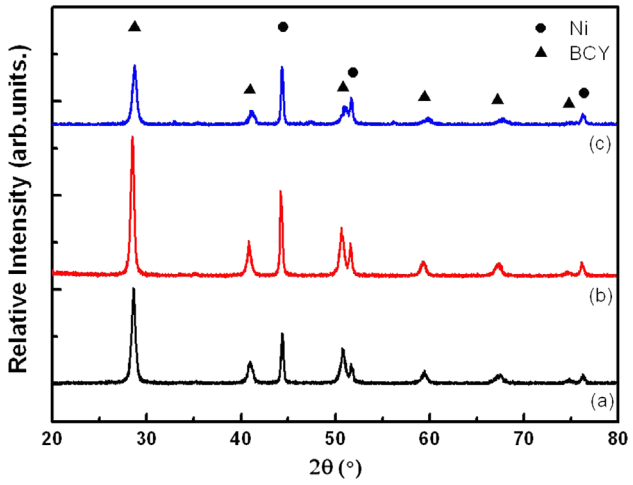

Fig. 8. X-ray diffraction patterns of Ni–BCY cermets after they had been reduced at 800 °C for 2 h: (a) Ni30–BCY70, (b) Ni35–BCY65, and (c) Ni40–BCY60.

consisted of a mixture of single-phase Ni and BCY. Furthermore, we found that there was no significant peak shift in 2θ values corresponding to the BCY peaks of the cermet powders, indicating that the Ni phase had not been incorporated into the BCY lattice. These results also suggested that an excrescent reaction did not take place during the preparation of the cermets and were indicative of the high chemical compatibility between BCY and Ni.

3.2. Microstructures and electrical characteristics of the Ni–BCY cermets

To determine the optimum temperatures for sintering the cermet membranes, the sintering behaviors of all the Ni–BCY composite powders were analyzed with a dilatometer. The results of the analyses showed that in the initial stages of the sintering process, the Ni–BCY composite powders exhibited

shrinkage behaviors similar to that of single-phase BCY. This was because in the initial stages, sintering was mainly controlled by the shrinking of the BCY phase that was present on the surface of the Ni phase. However, the rate of shrinkage increased at temperatures close to 1200 °C where the various fragments of the Ni phase connecting together. Furthermore, the total shrinkage increased with an increase in the Ni content. This was because the Ni powder which was fine and uniformly distributed sintered at a higher rate. On the basis of these results, the sintering temperature for the membranes of the Ni–BCY composites was fixed at 1400 °C, with all the sintered Ni–BCY membranes exhibiting a sufficiently high density (> 98%) that was dense enough to prevent gas leakage through a cermet membrane. Fig. 9 shows the XRD patterns of sintered pellets of the Ni–BCY composites. After being sintered at 1400 °C for 10 h the sintered disks exhibited distinct crystalline BCY and Ni phases, with no secondary phase being present.

Fig. 10 shows backscattered electron (BSE) images of cross-sections of sintered pellets of the Ni–BCY composites containing Ni in different concentrations. The BSE image of a sintered pellet of a Ni–BCY composite (Ni40–BCY60) not subjected to high-energy milling is also shown for comparison. In the images shown, the gray color represents the Ni phase, the white color the BCY phase, and the black color the pores in the pellets. As can be noticed, the Ni phase did not coagulate and was in instead distributed rather finely and evenly in the milled samples of all three compositions, in contrast to the unmilled one. Moreover, the Ni phase was more finely distributed in the cermets with a higher Ni content which would be more favorable to secure the Ni phase connectivity in composite membrane.

In order to determine the degree to which connections were formed in the Ni phases of the Ni–BCY composite membranes, we measured the total electrical conductivities of the cermets as a function of temperature. Fig. 11 shows the total electrical conductivities of the Ni–BCY composites measured in a mixture of wet 4% hydrogen/balance helium; these conditions were the same as those for the permeation tests. The conductivity of the perovskite BCY is also shown for comparison. As can be seen from the figure, there was a significant difference in the magnitudes and temperature dependence of the electrical conductivities of the 35, 35, and 40 vol% is Ni–BCY composites. The conductivity of the cermet with 40 vol% Ni was much higher than that of the other compositions. In addition, the conductivity of this particular cermets (40 vol% Ni) decreased with an increase in the temperature that is the typical metallic conduction behavior. On the other hand, the conductivities of the cermets with 30 and 35 vol% Ni were lower and similar to that of single-phase BCY. This indicated that the Ni connectivity in the cermets with 30 and 35 vol% was not sufficient to make the sufficient Ni connectivity and to allow for percolation. Hence, the results suggested that our original goal of inducing the formation of additional electronic pathways in the Ni phase was not met in the cermets with lower (30 and 35 vol%) Ni contents.

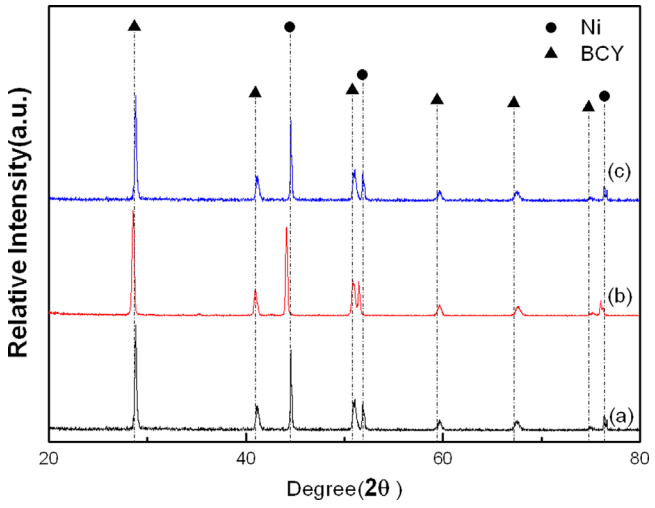

Fig. 9. X-ray diffraction patterns of cermet bulks after they had been sintered at 1400 °C: (a) Ni30–BCY70, (b) Ni35–BCY65, and (c) Ni40–BCY60.

3.3. Hydrogen permeation property of Ni–BCY cermet membranes

At the bulk diffusion controlled region, the hydrogen permeation flux though a cermet membranes such as Ni–BCY can be derived using the chemical diffusion model [35,39]. Because the diffusion of atomic hydrogen through the Ni phase is also possible, the total hydrogen flux can be expressed as the sum of the ambipolar and atomic diffusions while assuming that the oxygen potential gradients do not influence the transport of hydrogen across the membrane. Thus, the total hydrogen flux is given by

$$J_{H_2} = -\left(\frac{\chi RT}{4F^2L}\int_{P_{H_2}^{sweep}}^{P_{H_2}^{feed}} \frac{\sigma_{OH_O^\bullet}\sigma_{e'}}{\sigma_{OH_O^\bullet}+\sigma_{e'}} d\ln p_{H_2} + (1-\chi)\frac{\phi}{L}P_{H_2}^{\frac{1}{2}}\right) \quad (1)$$

where σ_i is the partial conductivity (i=$OH_O^\bullet$, $V_O^{\bullet\bullet}$ or e'), L is the thickness of the membrane, F is the Faraday constant, $d \ln p_{H_2}$ is the chemical potential gradient of hydrogen across the oxide membrane, χ is the volume fraction of the oxide phase, and Φ is the hydrogen permeability of Ni. Using the above-described model for the functioning of a hydrogen permeation membrane, we investigated the hydrogen permeation property of the various cermet membranes in terms of the various parameters influencing Eq. (1), such as the compositions, microstructures, and thicknesses of the membranes, as well as the hydrogen partial pressure during the permeation tests.

As mentioned previously, we investigated the relation between the Ni concentrations of the various cermets and the total electrical conductivities of the membranes formed using them. When the volume ratio of Ni in a cermet was increased, the cross-sectional area available for the flow of electrons also increased, resulting in an increase in the total electrical conductivity of the corresponding membrane. However, this increase in the total conductivity was not linearly proportional to the Ni concentration and increased abruptly when the Ni

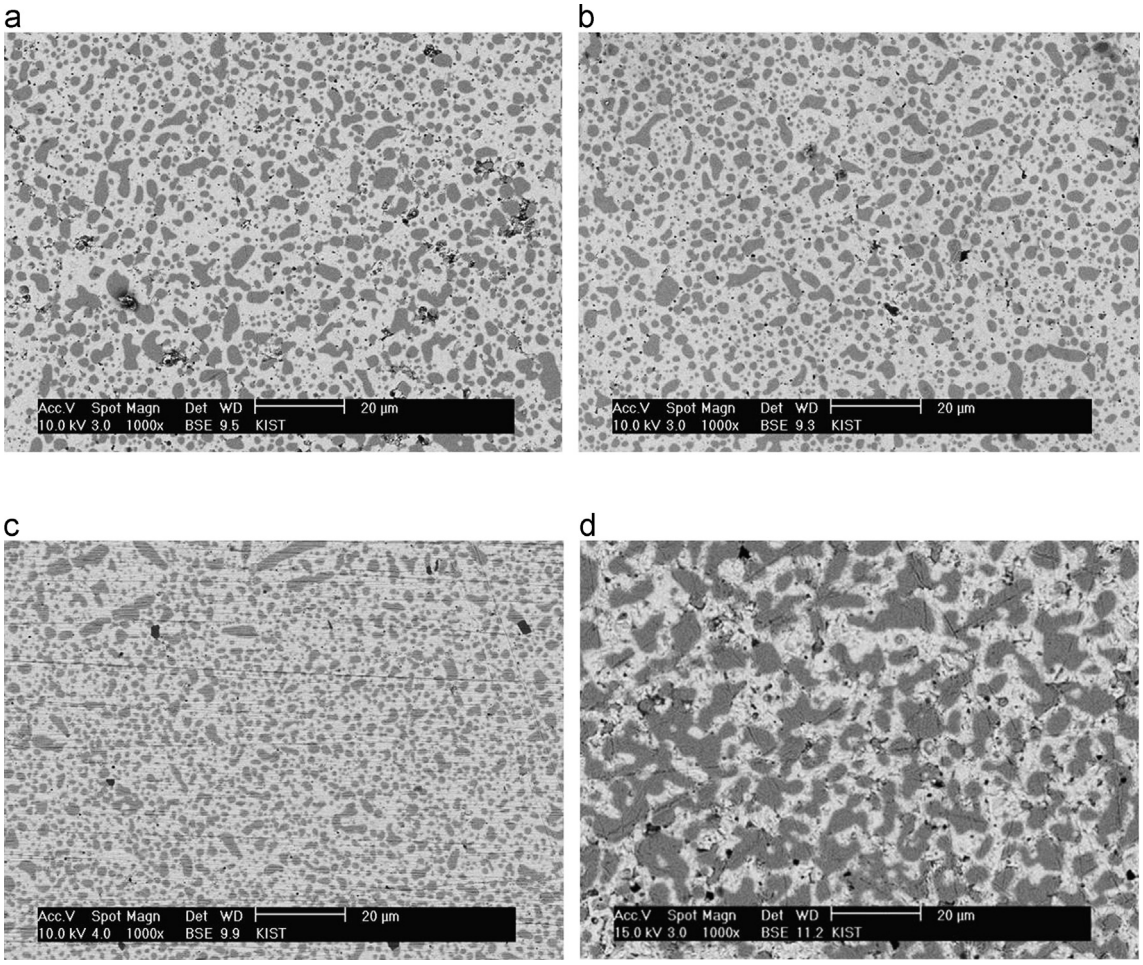

Fig. 10. Backscattered electron images of cermet membranes after they had been sintered at 1400 °C for 10 h: (a) Ni30–BCY70, (b) Ni35–BCY65, (c) and Ni40–BCY60. Figure (d)a Ni40–BCY60 membrane formed from a powder sample that had not been subjected to high-energy milling.

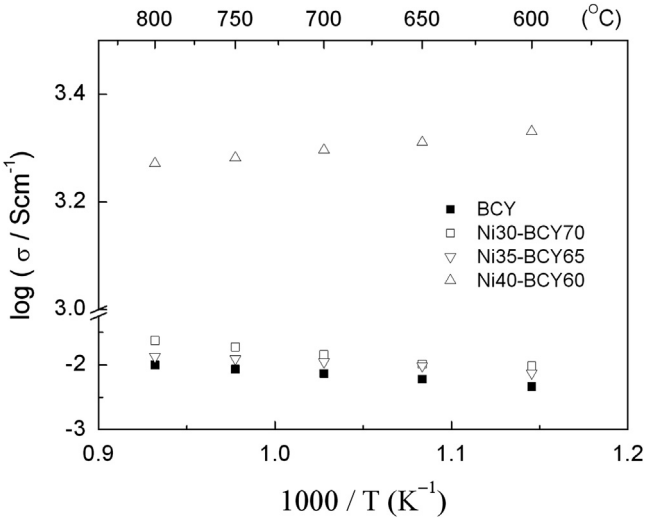

Fig. 11. Total electrical conductivities of BCY and various Ni–BCY cermets in a wet 4% hydrogen/balance He atmosphere.

phase percolated. Thus, the conductivity of a cermet membrane is an important indicator that can not only predict the magnitude of the hydrogen permeation flux attainable using the membrane but can also help elucidate the mechanism underlying hydrogen permeation through the membrane.

Thus, the hydrogen permeation fluxes of a series of Ni–BCY membranes with a thickness of 0.4 mm were measured over temperatures of 700–800 °C using a mixture of 4 mol% H_2/balance He as the feed gas and a mixture of 100 ppm H_2/balance N_2 as the sweep gas. As shown in Fig. 12, the hydrogen permeation flux of every Ni–BCY membrane increased with the temperature over temperatures of 700–800 °C regardless of the compositions of the membranes. Furthermore, the hydrogen permeation flux of each membrane increased with an increase in its Ni concentration. According to the results of the permeation tests, the rate of permeation through the membrane containing 40 vol% Ni was approximately 2.5 times higher than that through the membrane containing 35 vol% Ni. This was true over the entire range of temperatures tested. This increase in the hydrogen permeation flux can be attributed to the additional ambipolar permeation of hydrogen through the cermet membrane owing to the connections in the Ni phase. This was already verified by the fact that the total conductivity of the membrane of the cermet containing 40 vol% Ni was the highest. On the other hand, the other cermets exhibited permeability similar to that of a single-

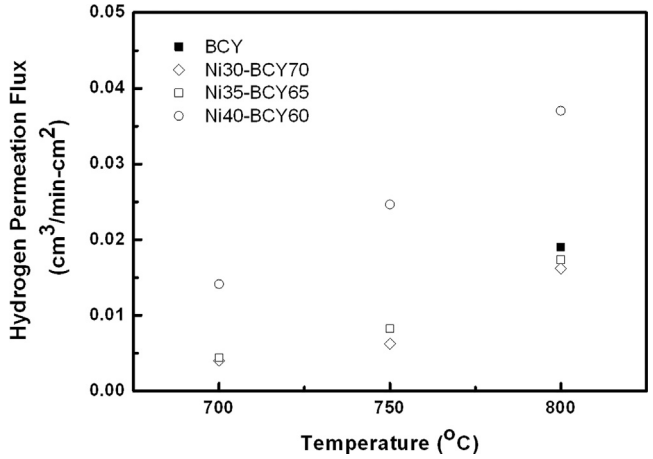

Fig. 12. Hydrogen permeation fluxes of Ni–BCY cermet membranes as a function of temperature.

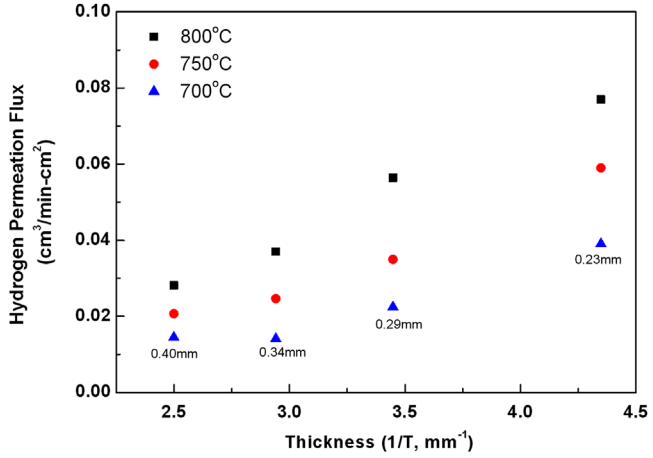

Fig. 13. Hydrogen permeation fluxes of Ni40–BCY60 cermet membranes of various thicknesses as a function of temperature.

phase BCY membrane. This indicated that the metallic phase did not contribute to the improvement in the electronic conduction of the Ni–BCY cermet membranes.

The effect of the thickness of the Ni40–BCY60 cermet membrane on its hydrogen permeability was studied. As shown in Fig. 13, the hydrogen permeation fluxes of all the samples, which had different thicknesses, increased with the temperature. In addition, for a given temperature, the hydrogen permeation fluxes of the membranes also increased with a decrease in the membrane thickness. Because the characteristic thickness of a cermet membrane is given by $Lc = D^*/k$, where k is the surface-exchange coefficient and D^* is the tracer diffusion coefficient, the thickness of the membrane determines whether the flux is limited by the bulk diffusion or by the dissociation reaction that takes place at its surface [40]. According to Zhang et al. [41], in the case of thinner membranes, the surface resistance makes up most of the total resistance, whereas the bulk resistance accounts for most of the total resistance in thicker membranes. In our case, even though the membranes were fairly thin, with the surface reaction expected to control the overall permeation process, the results in Fig. 13 indicated that permeation was, in

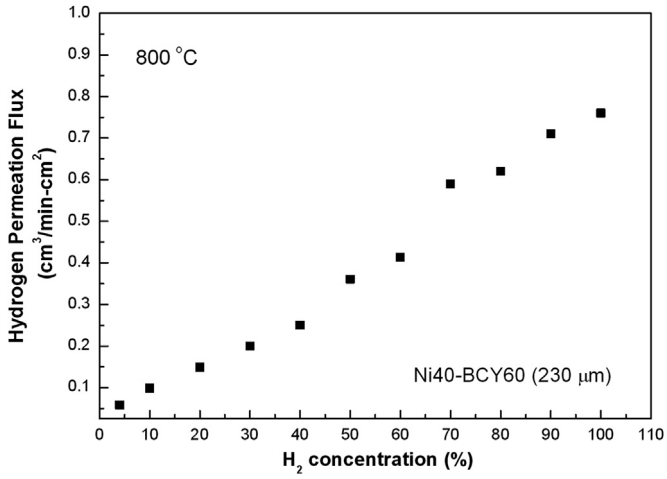

Fig. 14. Hydrogen permeation flux of a Ni40–BCY60 cermet membrane (thickness ~230 μm).

fact, controlled by bulk diffusion. However, because the linear extrapolation of the reciprocal thickness dependencies of hydrogen flux does not cross the origin, we still can't neglect the limited dissociation reaction at the surface of thinner membranes.

Fig. 14 shows the hydrogen permeation flux values of a 230-μm-thick cermet membrane for different hydrogen concentrations in the feed gas with the concentration of the sweep-side gas remaining constant. As can be seen from the figure, the hydrogen flux increased with an increase in the hydrogen partial pressure on the feed side. This result can be explained on the basis of an increase in the driving force for hydrogen transport, as well as by the increased conductivity of the membrane with respect to electrons, holes, and protons. Increasing the hydrogen partial pressure on the feed side increased the net driving force for hydrogen permeation and also increased the concentration of protons and electrons on the feed side. This resulted in an increase in the overall protonic and electronic conductivity of the membrane.

4. Conclusions

Fine-grained, dense membranes of the cermets Ni–Ba$(Ce_{0.9}Y_{0.1})O_{3-\delta}$ (or Ni–BCY) with excellent mixing homogeneity and improved Ni phase connectedness could be fabricated via the high-energy milling of composite powders containing Ni and BCY phases. In these controlled Ni–BCY cermet membranes, the Ni phase exhibited a higher degree of connectedness. As a result, the membranes exhibited higher total conductivities and thus promote nongalvanic hydrogen permeation owing to the ambipolar diffusion of protons and electrons. The results of hydrogen permeation tests performed on cells made of the cermets containing Ni in different concentrations showed that the cermet membrane containing BCY and 40 vol% Ni (Ni40–BCY60) exhibited the highest hydrogen permeation flux. Furthermore, the results of hydrogen permeation tests performed on membranes of varying thicknesses (230–400 μm) showed that the highest hydrogen permeation flux (0.76 $cm^3/(min\ cm^2)$) was noticed in the case of the thinnest (230-μm thick) Ni40–BCY60 membrane. This

indicated that the hydrogen permeation process was mainly controlled by bulk diffusion through the membrane rather than by reactions that took place at its surface.

Acknowledgment

This research was supported by the Fusion Research Program for Green Technologies through the National Research Foundation of Korea (NRF), funded by the Ministry of Education, Science and Technology (2011-00019297) and in part by the Institutional Research program of the Korea Institute of Science and Technology (KIST).

References

[1] Analysis of Effectiveness of the DOE Hydrogen Program, Hydrogen Technical Advisory Panel (HTAP), National Hydrogen Association, Washington, DC, 1998.
[2] M. Ricci, P. Bellaby, R. Flynn, What do we know about public perceptions and acceptance of hydrogen? A critical review and new case study evidence, International Journal of Hydrogen Energy 33 (2008) 5858–5880.
[3] D. Ipsakis, S. Voutetakis, P. Seferlis, F. Stergiopoulos, C. Elmasides, Power management strategies for a stand-alone power system using renewable energy sources and hydrogen storage, International Journal of Hydrogen Energy 34 (2009) 7081–7095.
[4] S. Yun, S.T. Oyama, Correlations in palladium membranes for hydrogen separation: a review, Journal of Membrane Science 375 (2011) 28–45.
[5] J.W. Phair, S.P.S. Badwal, Review or proton conductors for hydrogen separation, Ionics 12 (2006) 103–111.
[6] S.G. Chalk, P.G. Patil, S.R. Venkateswaran, The new generation of vehicles: market opportunities for fuel cells, Journal of Power Sources 61 (1996) 7–13.
[7] A.L. Dicks, Hydrogen generation from natural gas for the fuel cell systems of tomorrow, Journal of Power Sources 61 (1996) 113–124.
[8] J.P. Lange, Methanol synthesis: a short review of technology improvements, Catalysis Today 64 (2001) 3–8.
[9] B.A. Peppley, J. Amphlett, L.M. Kearns, R.F. Manm, Methanol-steam reforming on Cu/ZnO/Al2O3 catalysts. Part 2. A comprehensive kinetic model, Applied Catalysis 179 (1999) 31–49.
[10] National Hydrogen Association, A practical hydrogen development strategy, 1990, 3.
[11] J.M. Abrardo, V. Khuran, Hydrogen technologies to meet refiners' future needs, Hydrocarbon Proceeding 74 (1995) 43–49.
[12] G.Q. Li, R. Govind, Separation of oxygen from air using coordination complexes: a review, Industrial and Engineering Chemistry Research 33 (1994) 755–783.
[13] S. Uemiya, State-of-the-art of supported metal membranes for gas separation, Separation and Purification Methods 28 (1999) 51–85.
[14] C. Zuo, S.E. Dorris, U. Balachandran, M. Liu, Effect of Zr-doping on the chemical stability and hydrogen permeation of the Ni–$BaCe_{0.8}Y_{0.2}O_{3-\delta}$ mixed protonic–electronic conductor, Chemistry of Materials 18 (2006) 4647–4650.
[15] D. Gielen, G. Simbolotti, Prospects for Hydrogen and Fuel Cells, OECD Publishing, Paris, 2005.
[16] K. Coulter, Cost-effective method for producing self-supporting Pd alloy membrane for use in the efficient production of coal-derived hydrogen, DOE Hydrogen Program (2008).
[17] J. Okazaki, T. Ikeda, D.A.P. Tanaka, T.M. Suzuki, F. Mizukami, In situ high-temperature X-ray diffraction study of thin palladium/α-alumina composite membranes and their hydrogen permeation properties, Journal of Membrane Science 335 (2009) 126–132.
[18] C. Zuo, Doping and defect structure of mixed conducting ceramics for gas separation, (Doctoral thesis) Georgia Institute of Technology, 2006.
[19] S. Benson, Ceramics for advanced power generation, IEA clean coal centre reference, CCC/37, ISBN: 92-9029-349-7, 2000, pp 64.
[20] U. Balachandran, B. Ma, P.S. Maiya, R.L. Mieville, J.T. Dusek, J.J. Picciolo, J. Guan, S.E. Dorris, M. Liu, Development of mixed-conducting oxides for gas separation, Solid State Ionics 108 (1998) 363–370.
[21] H. Iwahara, Techological challenges in the application of proton conducting ceramics, Solid State Ionics 77 (1995) 289–298.
[22] T. Schober, F. Krug, W. Schilling, Criteria for the application of high temperature proton conductors in SOFCs, Solid State Ionics 97 (1997) 369–373.
[23] Z. Wu, M. Liu, Modelling of ambipolar transport properties of composite mixed ionic–electronic conductors, Solid State Ionics 93 (1997) 65–84.
[24] S.J. Song, E.D. Wachsman, J. Rhodes, S.E. Dorris, U. Balachandran, Numerical modeling of hydrogen permeation in chemical potential gradients, Solid State Ionics 164 (2003) 107–116.
[25] H. Matsumoto, T. Shimura, T. Higuchi, H. Tanaka, K. Katahira, T. Otake, T. Kudo, K. Yashiro, A. Kaimai, T. Kawada, J. Mizusaki, Protonic-electronic mixed conduction and hydrogen permeation in $BaCe_{0.9-x}Y_{0.1}Ru_xO_{3-\alpha}$, Journal of The Electrochemical Society 152 (2005) 488–492.
[26] J. Guan, S.E. Dorris, U. Balachandran, M. Liu, Solid State Ionics 100 (1997) 45–52.
[27] J. Guan, S.E. Dorris, U. Balachandran, M. Liu, The effects of dopants and A:B site nonstoichiometry on properties of perovskite-type proton conductor, Journal of The Electrochemical Society 145 (1998) 1780–1786.
[28] J. Guan, S.E. Dorris, U. Balachandran, M. Liu, Development of mixed-conducting membranes for hydrogen separation, Ceramic Transactions 92 (1998) 1–12.
[29] G. Zhang, S.E. Dorris, U. Balachandran, M. Liu, Interfacial resistances of Ni–BCY mixed-conducting membranes for hydrogen separation, Solid State Ionics 159 (2003) 121–134.
[30] U. Balachandran, T.H. Lee, S. Wang, C. Zuo, S.E. Dorris, K.S. Rothenberger in: Proceeding of the 20th International Pittsburgh Coal Conference, 46, 2003, 187.
[31] U. Balachandran, T.H. Lee, G. Zhang, S.E. Dorris, K.S. Rothenberger, B. H. Howard, B. Morreale, A.V. Cugini, R.V. Siriwardane, J.A. Poston Jr., and E.P. Fisher, in: Proceedings of the 26th International Technical Conference on Coal Utilization and Fuel Systems,Clearwater Coal Technical Association, Gaithersburg, 2001 pp. 751–761.
[32] C. Suryanarayana, Mechanical alloying and milling, Progress in Materials Science 46 (2001) 1–184.
[33] T.A.G. Restivo, S.R. de Mello-Castanho, Nickel–Zirconia cermet processing by mechanical alloying for solid oxide fuel cell anodes, Journal of Power Sources 185 (2008) 1262–1266.
[34] H. Kim, K. Ahn, B. Kim, J. Lee, Y.-C. Chung, H.-R. Kim, J.-H. Lee, Improved microstructural homogeneity of Ni–BCY cermets membrane via high energy milling, Journal of the Korean Ceramic Society 49 (2012) 648–653.
[35] S.-J. Song, J.-H. Moon, T.-H. Lee, S.E. Dorris, U. Balachandran, Thickness dependence of hydrogen permeability for Ni–$BaCe_{0.8}Y_{0.2}O_{3-\delta}$, Solid State Ionics 179 (2008) 1854–1857.
[36] V.F. Kiselev, O.Y. Krylov, Adsorption and Catalysis on Transition Metals and their Oxides, Spring-Verlag, Berlin, Germany, 1989.
[37] V. Agarwal, M. Liu, Electrochemical properties of $BaCe_{0.8}Gd_{0.2}O_3$ electrolyte films deposited on Ni–$BaCe_{0.8}Gd_{0.2}O_3$ substrates, Journal of The Electrochemical Society 144 (1997) 1035–1040.
[38] F.S. Galasso, Structure, Properties and Preparation of Perovskite-type Compounds, 1st edition, Pergamon Press, Oxford, England, 1969.
[39] S.-J. Song, J.-H. Moon, H.-S. Park, S.E. Dorris, U. Balachandran, Fast proton conduction path in Ni–$BaCe_{0.8}Y_{0.2}O_{2.9-\delta}$ membrane, Ionics 14 (2008) 37–42.
[40] J. Siman, in: A.F. Sammells, M.V. Mundschau (Eds.), Nonporous Inorganic Membranes, Willy-VCH, Germany, 2006, p. 175.
[41] G. Zhang, S. Dorris, U. Balachandran, M. Liu, Effect of Pd coating on hydrogen permeation of Ni–Barium Cerate mixed conductor, Electrochemical and Solid-State Letters 5 (2002) 5–7.